

Evaluation of Ocean Currents Observed from Autonomous Surface Vehicles

BENJAMIN A. HODGES,^a LAURENT GRARE,^b BENJAMIN GREENWOOD,^a KAYLI MATSUYOSHI,^b NICK PIZZO,^b
NICHOLAS M. STATOM,^b J. THOMAS FARRAR,^a AND LUC LENAIN^b

^a Woods Hole Oceanographic Institution, Woods Hole, Massachusetts

^b Scripps Institution of Oceanography, University of California, San Diego, La Jolla, California

(Manuscript received 10 May 2023, in final form 17 August 2023, accepted 23 August 2023)

ABSTRACT: The development of autonomous surface vehicles, such as the Boeing Liquid Robotics Wave Glider, has revolutionized our ability to collect surface ocean–lower atmosphere observations, a crucial step toward developing better physical understanding of upper-ocean and air–sea interaction processes. However, due to the wave-following nature of these vehicles, they experience rapid shifting, rolling, and pitching under the action of surface waves, making motion compensation of observations of ocean currents particularly challenging. We present an evaluation of the accuracy of Wave Glider–based ADCP measurements by comparing them with coincident and collocated observations collected from a bottom-mounted ADCP over the course of a week-long experiment. A novel motion compensation method, tailored to wave-following surface vehicles, is presented and compared with standard approaches. We show that the use of an additional position and attitude sensor (GPS/IMU) significantly improves the accuracy of the observed currents.

KEYWORDS: Currents; In situ oceanic observations; Instrumentation/sensors

1. Introduction

Submesoscale dynamics contribute significantly to vertical transport of carbon and other climatologically and biologically important variables in the upper ocean (e.g., McWilliams 2016; D’Asaro et al. 2018). These vertical fluxes modulate ocean–atmosphere exchange, but our observational knowledge of them is limited by the notorious difficulty of measuring the vertical component of ocean currents directly. One strategy we are pursuing to address this challenge as part of the NASA Sub-Mesoscale Ocean Dynamics (S-MODE) program (Farrar et al. 2020) is to estimate the horizontal divergence of the horizontal velocity field, inferring the vertical current indirectly. At the submesoscale, these velocity gradients are on the same order of magnitude as the Coriolis frequency, f . In subtropical latitudes, then, resolving vorticity and divergence over spatial scales of about 1 km requires distributed current observations with accuracy of about 1 cm s^{-1} . This need has motivated us to carefully consider the random and systematic errors that arise in velocity measurements collected from a broad range of instruments and platforms used during S-MODE.

Wave Gliders (Boeing Liquid Robotics) are autonomous surface vehicles that extract energy for propulsion from ocean waves (e.g., Hine et al. 2009; Lenain and Melville 2014; Grare et al. 2021). These platforms are well suited to ocean current observation at the submesoscale as they can be operated in tight arrays and be piloted to interesting oceanic features, while providing ample power to run instruments like acoustic Doppler current profilers (ADCPs).

Achieving accuracy of $O(1 \text{ cm s}^{-1})$ in ADCP observations collected from Wave Gliders requires careful motion compensation because surface waves cause the platforms to undulate at $O(1 \text{ m s}^{-1})$ and rotate unpredictably (for reference, the nominal instrumental noise for the Wave Glider ADCP’s as configured, in the absence of any external sources of error, was 0.36 cm s^{-1} for a 10-min ensemble average current profile). One standard method by which this compensation can be carried out relies on a fluxgate compass and tilt sensor to establish the orientation of the platform (allowing rotation of the observed current vectors into a fixed reference frame), and GPS positions to infer its average horizontal velocity over the collection period of an ensemble of ADCP pings (which, added to the corresponding ensemble average current relative to the instrument, yields the estimated current profile). Amador et al. (2023) provide an evaluation of Wave Glider current measurements made following this procedure. Alternatively, the 3D position, rotation, velocity, and orientation of the platform can be estimated at fine temporal resolution (here, 20 Hz) using a GNSS-aided dual-antenna inertial measurement unit (GPS/IMU), which combines inputs from 3-axis accelerometers and gyros with those from two spatially separated GPS antennas via a Kalman filter to produce an “inertial solution” for the platform motion. Combination of satellite transmissions received at the two antennas enables a more accurate measurement of true heading than can be achieved with a magnetometer, and the inertial solution is able to distinguish between changes in attitude and lateral accelerations that would be conflated by a solitary tilt sensor. The enhanced accuracy—particularly on short time scales—of platform motion observations obtained by this method make it feasible to fully motion-correct the velocity samples for each ping prior to forming an ensemble average. In this work, we characterize the accuracy of ADCP measurements made from Wave Gliders and we examine the success of different methods of motion correction by comparing the resulting velocity observations

 Denotes content that is immediately available upon publication as open access.

Corresponding author: Ben Hodges, bhodges@whoi.edu

DOI: 10.1175/JTECH-D-23-0066.1

© 2023 American Meteorological Society. This published article is licensed under the terms of the default AMS reuse license. For information regarding reuse of this content and general copyright information, consult the AMS Copyright Policy (www.ametsoc.org/PUBSReuseLicenses).

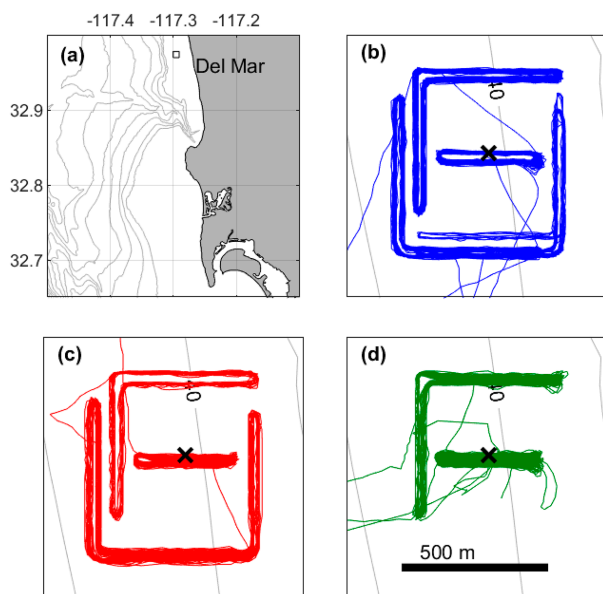


FIG. 1. (a) San Diego, California, and coastal waters, with 100-m isobaths in gray and the experiment operational area indicated by a black-outlined box near the top. Also shown are magnified views of the black-outlined box interior showing the location of the Sea Spider (black cross), 10-m isobaths, and the tracks of the three Wave Gliders: (b) WHOI43 in blue, (c) Stokes in red, and (d) Planck in green.

with those made with a bottom-mounted ADCP over the course of a week-long experiment.

2. Experiment and instrumentation

a. Operations

Working from the R/V *Beyster* on 4 March 2021, we deployed an ADCP on a bottom tripod approximately 2 km from shore near Del Mar, California, in 40 m of water (Fig. 1). The site was chosen as deep as possible while remaining easily accessible to scuba divers so as to maximize the number of range bins of velocity data. The bottom tripod, an RDI/Teledyne Sea Spider, carried an upward-looking 600-kHz RDI Workhorse ADCP. Divers ensured that the ADCP was level. The position was recorded as latitude $32^{\circ}58.450'N$, longitude $117^{\circ}17.718'W$. The ADCP was configured to sample at 1 Hz with 2-m range bins. An RBR Concerto CTD mounted on the tripod logged pressure, temperature, and conductivity at 5-min intervals.

Three SV3 Wave Gliders were then deployed from the R/V *Beyster*. We will refer here to the following Wave Glider components (see Fig. 2): the “float” is the kayak-like surface expression of the vehicle; the “sub” is the winged subsurface component that hangs from the float, providing the propulsion and steering; and the “umbilical” is the faired tether connecting the float and sub. The three Wave Gliders are named Planck, Stokes, and WHOI43. The science payloads were configured following a design developed at the Air–Sea Interaction Laboratory, Scripps Institution of Oceanography (SIO; Grare et al. 2021). Each Wave Glider carried two ADCPs:

a 300-kHz RDI Workhorse Monitor mounted in the float looking downward (transducer depth ~ 0.2 m), and a Nortek Signature1000 mounted on the sub looking upward (depth ~ 8.5 m). The RDIs were configured to sample at 1 Hz using 2-m depth bins; the Norteks sampled at 8 Hz and used a combination of 0.25- and 0.5-m depth bins for evaluation purposes. Analysis of the Nortek ADCPs is not included here. Each Wave Glider also had a dual-antenna GPS-aided IMU mounted on the float, providing position, orientation, velocity, and angular velocity estimates at 20 Hz; this allowed correction of the RDI currents (and also the measured winds) for platform motion. The SIO vehicles—Planck and Stokes—carried Novatel OEM7720 dual-antenna receivers combined with a Epson EG320N IMU, while WHOI43 used a Vectornav VN-300. Each system used a combination of two Campbell CR6 dataloggers to handle the recording and time stamping of incoming data as well as the generation of decimated real-time datasets for telemetry via the cellular and Iridium communication channels native to the Wave Glider.

All Wave Gliders carried the following additional sensors: a Gill R3-50 3D ultrasonic anemometer sampling at 20 Hz (mounted on the bow), a Vaisala WXT-530 and an Airmar 200-WX weather station sampling atmospheric properties at 1 Hz (mounted amidships), a GPS compass (Hemisphere V104 or equivalent Si-Tex model) sampling at 10 Hz, and a Sea-Bird GPCTD sampling water temperature and salinity at 1 Hz (mounted under the float). The SIO vehicles had PME T chains attached to their umbilicals, and high-frequency air pressure sensors on the float bows. The WHOI vehicle was equipped with Kipp and Zonen shortwave and longwave radiometers (SMP21 and SGR4, respectively) installed on a mast at the float stern, and an internally logging RBR Concerto with attached WETLabs fluorometer and transmissometer on the sub.

Initially each Wave Glider was dispatched to its own square holding pattern. Within a day, they transitioned to a coordinated pattern around the Sea Spider (Fig. 1): two of the vehicles would occupy L-shaped circuits along two edges of a 500-m square centered on the Sea Spider, and the third would transit back and forth along a 300-m east–west line (the “central transect”) directly over the Sea Spider (for practical reasons the pattern for this transect line was actually a 30-m-wide loop, traversed in the clockwise direction). To facilitate intercomparison between vehicles, they were cycled through these roles in turn, switching assignments every 1–3 days. Early on, the L-shaped circuits covered all four sides of the 500-m square, but once it became clear that acoustic interference from the seafloor echo was more pronounced in shallower water, the east side of the square was abandoned, with the two perimeter Wave Gliders following nonoverlapping circuits along the remaining three sides.

b. Environmental conditions

Winds during the experiment varied from light to moderate (Fig. 3a): for the first four days, calm periods punctuated typical wind speeds near 5 m s^{-1} ; the following two days were windier, mostly between 4 and 8 m s^{-1} ; the final day had a

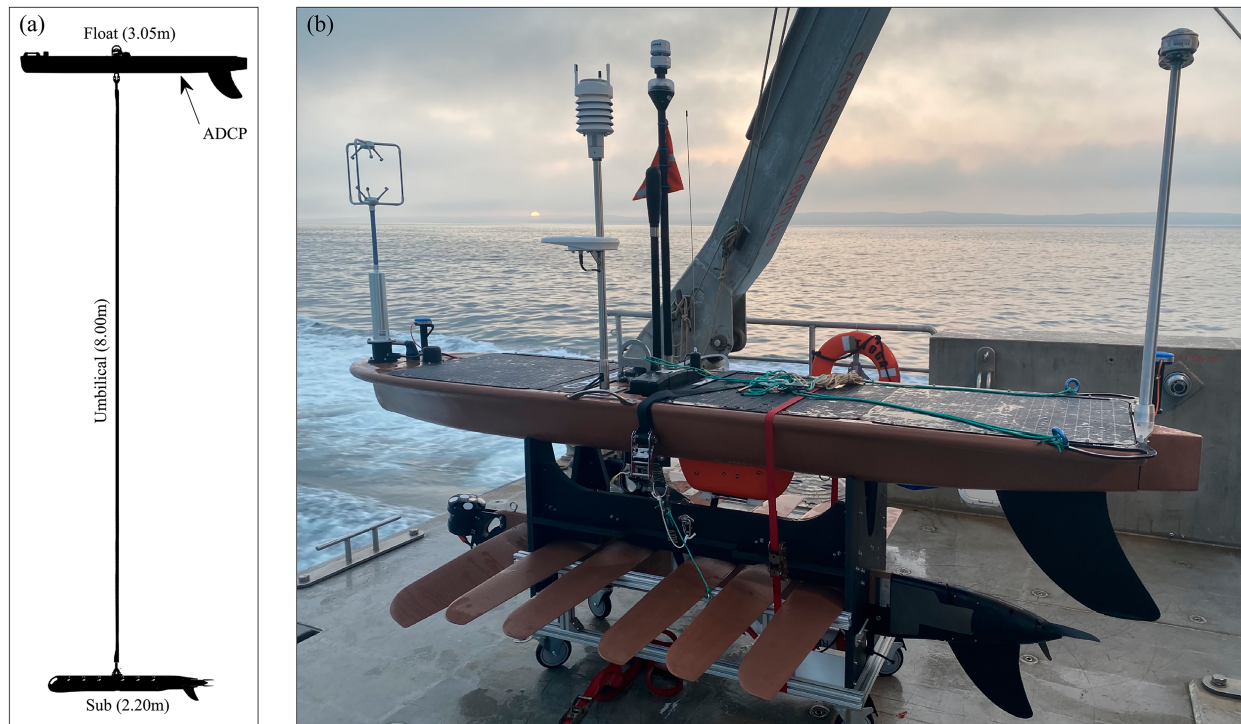


FIG. 2. (a) Schematic of an SV3 Wave Glider (reproduced with permission from Boeing Liquid Robotics), showing names and lengths of major components, and the location of the downward-looking RDI ADCP. (b) Wave Glider WHOI43 in its cradle on deck.

return to lower wind speeds. Wind direction (Fig. 3b) was variable; the stronger winds in the latter half of the experiment were mostly easterly.

The significant wave height H_s , initially below 1 m (Fig. 3c), increased to approximately 1.5 m over the course of 6 March, dominated by waves of approximately 15 s peak period T_p (Fig. 3d). Wave height decreased over 8 March, reaching a minimum of about 1 m, before increasing again on 9 March ($T_p \approx 6$ s), as winds strengthened. A maximum of 1.8-m significant wave height was reached early on 10 March.

Altogether, then, the sea state and winds during the deployment were representative of the calmer end of the spectrum of environmental conditions that might be expected during an extended midlatitude observation campaign. Our results are most applicable to this range of conditions. Wave Glider ADCP accuracy may deteriorate from that reported here in rougher sea states, but, given the short duration of our experiment, the relatively narrow range of environmental conditions spanned, the confounding variables of inherent differences among the three vehicles and changes in natural spatial variability, and the rapid growth of uncertainty with extrapolation, we are not yet able to confidently predict the details of this suspected dependence.

3. Methods

a. Sea Spider (bottom-mounted ADCP)

The bottom-mounted ADCP recorded velocities at 1 Hz in beam coordinates in 50 bins spanning a depth range of 2 m

each, with a blanking distance of 1 m. The raw binary record was converted to MATLAB format and transformed into Earth coordinates (east, north, and up) using the `rdradcp` package (<https://www.eoas.ubc.ca/~rich/RDADCP>). Velocity estimates were rejected as invalid based on the following criteria:

- 1) *Range*—Bins 20–50 corresponded to ranges beyond the sea surface, and were ignored, as were bins 18–19, due to severely deteriorating data quality near the surface. Thus, the shallowest usable velocities (bin 17) had depths of ~ 5 m.
- 2) *Error velocity*—The four ADCP beams are positioned every 90° around the axis of the instrument, slanted outward at 20° . Each pair of opposite beams produces an independent measurement of W , the current velocity component in the direction of the ADCP axis. The difference between these two estimates of W is defined as the “error velocity.” Velocity estimates were rejected if the corresponding error velocity magnitude was too large. For the first 14 range bins (deeper than ~ 10 m from the surface) the threshold was set at 0.05 m s^{-1} ; for the shallower bins (15–17), where wave motion was stronger, the threshold was increased to 0.1 m s^{-1} .
- 3) *Correlation*—For every observation, the ADCP records the correlation, a measure of the quality of the reflected acoustic signal. The recorded value is an integer ranging from 0 to 255. Here, velocity estimates for which the average correlation dropped below a value of 100 were rejected. One of the artifacts addressed by this step is the

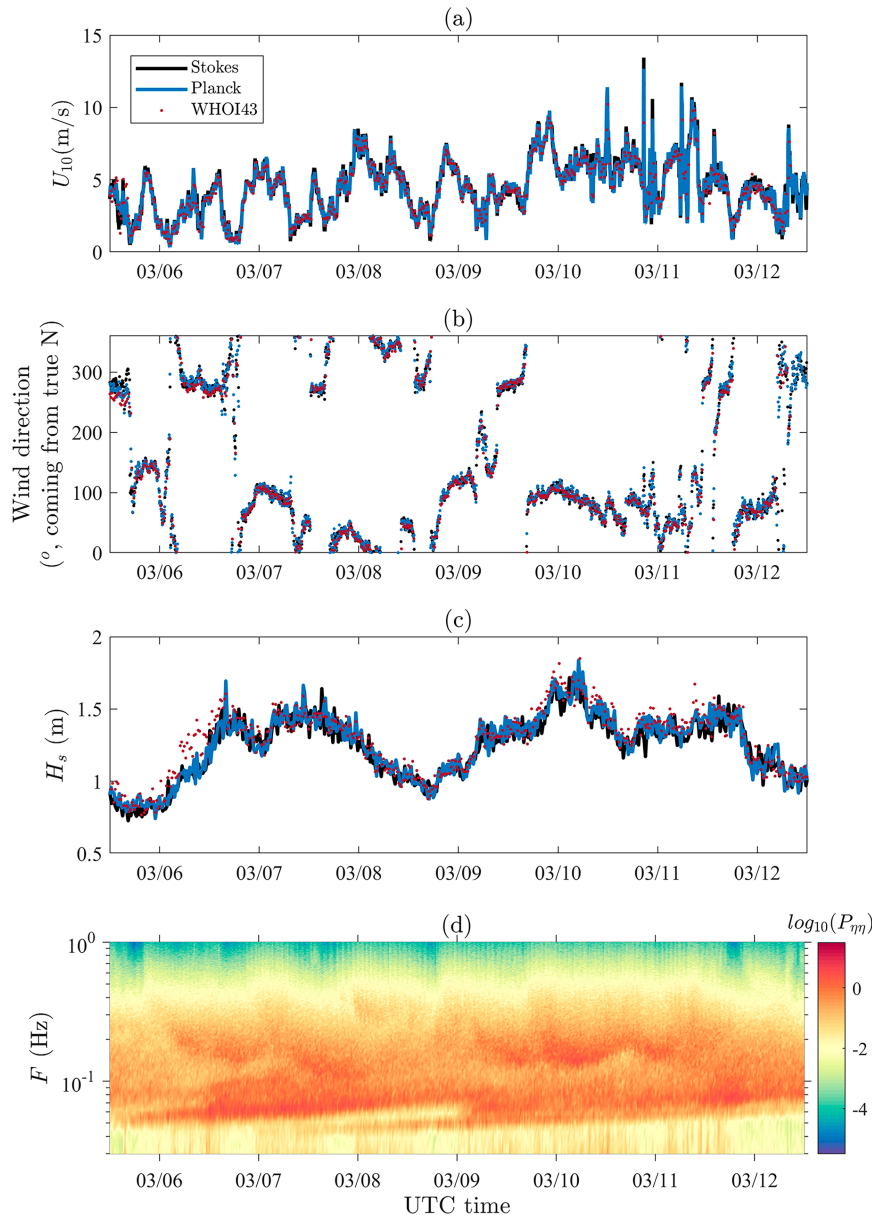


FIG. 3. Environmental conditions during the experiment, collected from the three Wave Gliders: (a) wind speed U_{10} , (b) wind direction, (c) significant wave height H_s , and (d) the wave spectrogram collected from Wave Glider Stokes. Note that the wind data from Wave Glider WHOI43 presented in (a) and (b) are real-time products, because of a failure of the internal recorder.

acoustic interference occasionally caused by the downward-looking 300 kHz ADCPs as they passed above the Sea Spider.

- 4) *Velocity*—Velocity outliers (estimates that fell outside the expected range at their depth) were thrown out. Specifically, for the near-surface bins (15–17) alongshore (i.e., meridional) velocity components with magnitudes greater than 2 m s^{-1} were rejected. For the remaining bins, northward velocities in excess of 0.53 m s^{-1} and southward velocities in excess of 0.63 m s^{-1} were rejected.

- 5) *Manual inspection*—Two instances, of ~ 2 -min duration each, of suspicious coherent structures in correlation, echo intensity, and/or velocity that were not screened out by other methods—for example, caused by schools of fish and other biological activities—were manually removed.

Following these quality-control steps, the current observations were rotated clockwise by a set angle of 11.2° into a true-north reference frame from a magnetic-north one. This angle was validated by confirming that it resulted in current

directions that matched, on average, those from the Wave Gliders (which obtain more accurate headings using the dual GPS).

To facilitate comparison with the Wave Glider-observed currents, the current profiles were mapped to a reference frame relative to the tidally varying sea surface, using the pressure record collected from the RBR Concerto that was mounted on the Sea Spider (the tidal range during the experiment was ~ 2 m, or one range bin). The timing of transitions of the surface between range bins obtained in this way was verified against the surface signature in echo intensity, ensuring that the range equated to a depth of zero was correctly identified.

b. Wave glider

1) VELOCITY PROCESSING

The downward-looking ADCPs mounted on the Wave Glider floats recorded velocities every second in a beam coordinate reference frame (50 bins spanning a depth range of 2 m each), with the first cell at 3.94-m depth. Velocity estimates were rejected as invalid based on a number of criteria: as the test was carried out in shallow water, only the upper 21 depth bins were retained; one disadvantage of Wave Gliders as a platform from which to collect surface-mounted ADCP observations is that the sub, at approximately 8-m depth, causes substantial acoustic interferences at ranges of both ~ 8 and ~ 16 m (the latter presumably due to a triple reflection producing the acoustic path ADCP-sub-surface-sub-ADCP) so data from bins 3, 4, 7, and 8 were removed; velocity estimates for which the 4-beam cumulative correlation fell below a designated threshold (475 of a possible 1020) were rejected; and finally, velocities with unreasonably large magnitudes (exceeding 1.5 m s^{-1} after motion correction) were rejected. The correlation and velocity magnitude rejection thresholds differ from those used in the processing of the bottom-mounted ADCP for a number of reasons: differences between the instruments themselves (i.e., the operating frequency—600 kHz for the bottom-mounted ADCP vs 300 kHz for the Wave Gliders) and differences between their operating environments (40-m depth vs floating on the surface) result in datasets with distinct attributes. In each case, the velocity magnitude thresholds are chosen by looking for a “kink” or sudden flattening in slope of the tail of the velocity distribution; the presumption is that the steeper slope is characteristic of the real velocity field, and the flatter one indicative of significant contamination by spurious values. Correlation thresholds are determined by examining the statistics of the associated velocities: with samples grouped by correlation, the threshold is chosen as the value below which the standard deviation of the corresponding velocities begins to increase significantly.

2) GPS/IMU PROCESSING AND SYNCHRONIZATION

The GPS/IMU data (three-dimensional position, velocity, orientation, and angular rate) were processed using Novatel Inertial Explorer software for the SIO Wave Gliders, using the precise point positioning postprocessing option. For the WHOI43 Wave Glider, after outlier removal, a 25-s rolloff

high-pass filter was applied to the vertical velocity record to remove a spurious long-term mean of $\sim 0.06 \text{ m s}^{-1}$.

The payload datalogger is synchronized to GPS and records accurately the time at which each ADCP ping data record is logged, so clock drift is not a concern when aligning ADCP and IMU; however, the raw records display a relative offset in time, due to the lag associated with the acoustic processing and the buffering of outgoing data streams within the ADCP. To determine this offset, the velocity of the ADCP along its axis was computed using the IMU and compared with the ADCP’s estimate of the corresponding component of the relative current—i.e., the current directly toward/away from the ADCP head. For all three vehicles, the correlation between these two records was maximum for a lag of seven 20-Hz IMU scans. Accordingly, the IMU records were set back by 0.35 s prior to rotation of the measured velocities into an Earth-coordinate frame and motion compensation.

3) DEPTH BIN MAPPING

As vertical shear is usually large relative to horizontal shear, it is sensible to consider ADCP returns from an equivalent depth along each beam to estimate the current vector at that depth; when the ADCP is tilted, that may mean combining beam velocities from different range bins. For each ping, the instantaneous angle of each beam is computed from the IMU pitch and roll; the along-beam velocities corresponding to all range bins that deviated from their nominal depths by at least half a bin were replaced by the velocity from the bin that was closest to that nominal depth. These beam velocities were then combined to form single-ping estimates of the current vector in instrument coordinates at each nominal depth.

4) CALIBRATION OF ADCP MOUNTING ORIENTATION

To minimize interference from the sub, the ADCP is not mounted with one pair of beams oriented forward/aft and the other port/starboard, but rather rotated 45° such that all four beams angle out to the sides. Beam 3 is “forward” by RDI convention and is positioned 45° counterclockwise from the bow of the Wave Glider, and therefore nominally the current vectors can be transformed from instrument coordinates to Wave Glider coordinates by a clockwise rotation of 45° . However, the relative orientation of the ADCP and IMU in the vehicle is not known precisely, so the actual required rotation is determined empirically by eliminating heading bias in the measured currents.

Depending on the setup, offset angles can change from one deployment to the next; for example, mounting holes may allow a small amount of variation in the final position of the instrument. While these biases are small for the roll and pitch angles [$O(0.1^\circ)$], the heading bias is not negligible [$O(1^\circ)$] and needs to be accounted for. Moreover, under typical conditions (float pitch and roll $\ll 90^\circ$), the error associated with a bias in roll or pitch angle maps into the Earth frame predominantly as a modification of the vertical component of the current, which we do not intend to resolve; a bias in heading, on the other hand, introduces errors primarily into the observations whose accuracy we are attempting to characterize—the east

and north components of the current. Accordingly, when establishing the relative orientation of the ADCP and IMU, we focus on the heading offset. The eastward and northward components of the error produced by this offset vary with heading, so minimizing the covariance of Wave Glider heading with the horizontal components of the measured current is one way to obtain a proper alignment calibration. The design of our experiment, with course changes every 5–10 minutes, is well suited to this method: the frequent shifts in heading provide an energetic signal with which to compare measured currents. Our method of determining the heading bias is to optimize the metric described below; intermediate data products corresponding to steps in the analysis are written as P_i^k where i signifies a horizontal component (east or north) of the current C , and k distinguishes between the various intermediate products. Time and depth variables are signified by t and z , respectively.

- 1) An artificial bias ϕ ranging from -4° to $+4^\circ$ in 0.1° increments was introduced to the IMU heading. Using this altered heading, observed currents were transformed into the Earth frame, generating time series $C_E(t, z, \phi)$ and $C_N(t, z, \phi)$ of the east and north current components for each depth bin.
- 2) For each current component, each bias, and each bin, 5-min running averages were computed:

$$P_i^1(t, z, \phi) = \langle C_i(t, z, \phi) \rangle_{\Delta T} \\ = \frac{1}{\Delta T} \int_{t-\Delta T/2}^{t+\Delta T/2} C_i(\tau, z, \phi) d\tau, \text{ with } \Delta T \equiv 5 \text{ min.} \quad (1)$$

- 3) For each current component and each bias, the 5-min running averages from depth bins 10 to 13 (i.e., from 22- to 28-m depths; this range of depths was chosen as it is comfortably below the acoustic interference from the sub and above that from the sea floor) were averaged together:

$$P_i^2(t, \phi) = \frac{1}{4} \sum_{j=10}^{13} P_i^1(t, z_j, \phi). \quad (2)$$

- 4) A 60-min running-standard deviation operator was applied to P_i^2 :

$$P_i^3(t, \phi) = \frac{1}{\Delta T^{1/2}} \sqrt{\int_{t-\Delta T/2}^{t+\Delta T/2} [P_i^2(\tau, \phi) - \langle P_i^2(\tau, \phi) \rangle_{\Delta T}]^2 d\tau}, \\ \text{with } \Delta T \equiv 60 \text{ min.} \quad (3)$$

- 5) The mean values of P_i^3 over the duration of the experiment were computed. The heading bias angle that minimized these mean values was chosen as the correct offset.

Using this method with the observations collected during this experiment, we found a heading calibration offset of 45.0° , 43.9° , and 46.7° for Wave Gliders Stokes, WHOI43, and Planck, respectively (the nominal value being 45°).

5) TRANSFORMING TO THE EARTH-COORDINATE FRAME

Three Euler-angle rotations in sequence¹ transform the relative current vectors (the measured velocity of the water relative to the ADCP) from ADCP coordinates into Earth coordinates: first the ADCP roll, then the pitch, and finally the heading. Thus,

$$\mathbf{U}'_{\text{meas}} = \mathbf{M}_h \mathbf{M}_p \mathbf{M}_r \mathbf{U}_{\text{meas}}, \quad (4)$$

where \mathbf{U}_{meas} is the measured velocity of the water relative to the ADCP, $\mathbf{U}'_{\text{meas}}$ is that relative velocity in the east–north–up coordinate frame, and \mathbf{M}_h , \mathbf{M}_p , and \mathbf{M}_r are the rotation matrices for heading, pitch, and roll, respectively.

The absolute current estimate \mathbf{U}_{WG} is then the vector sum of the relative current and the velocity of the ADCP:

$$\mathbf{U}_{\text{WG}} = \mathbf{U}'_{\text{meas}} + \mathbf{U}_{\text{ADCP}}. \quad (5)$$

The velocity of the ADCP, in turn, is the sum of the measured translational velocity of the IMU and the relative motion of the ADCP due to its displacement from the IMU and the instantaneous rotation rate of the Wave Glider:

$$\mathbf{U}_{\text{ADCP}} = \mathbf{U}_{\text{IMU}} + \boldsymbol{\omega} \times \mathbf{r}, \quad (6)$$

where $\boldsymbol{\omega}$ is the angular velocity vector of the platform and \mathbf{r} is the displacement vector of the ADCP relative to the IMU. These steps complete the transformation of the raw 1-Hz velocities in beam coordinate reference frame into the Earth-coordinate frame. An additional step, which was not implemented here but could be important when processing Wave Glider ADCP data collected in more energetic seas, is to assign a depth to each range bin, at each ping, according to the instantaneous vertical position of the ADCP, which rises and falls following the surface waves. Average current profiles would be obtained over range bins that correspond to a particular depth below the mean surface level. Assigning the vertical coordinate of the single-ping velocity estimates in this way should eliminate a Stokes-drift-like bias in the ensemble average current that is expected in a surface following reference frame (Pollard 1973; Amador et al. 2017).

4. Results

In this section we examine the difference between concurrent velocity measurements collected from the bottom-mounted ADCP and from the Wave Gliders. These records contain contributions from surface waves (i.e., orbital motion), which, in the context of this comparison, are treated as noise; to reduce this effect, we average the 1-Hz observations with a 10-min averaging window, which suppresses the surface wave signal reasonably well.

¹ Sample MATLAB transformation code that can be used to transform ADCP velocities to Earth's reference frame using GPS/IMU can be found online (https://smode.whoi.edu/BTMA_2021/index.html).

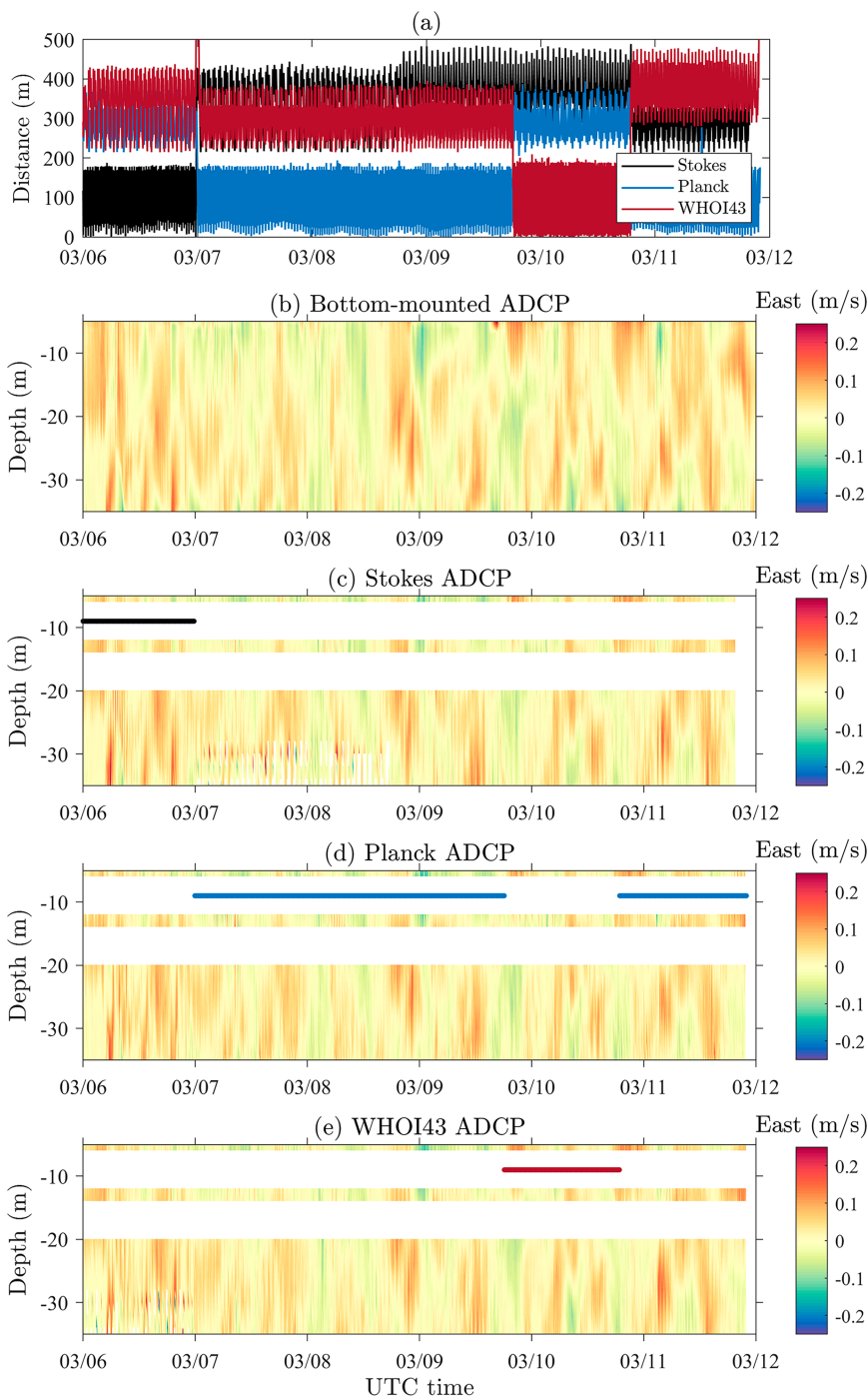


FIG. 4. (a) Distance between each vehicle and the bottom-mounted ADCP. Also shown is the east component of the current (10-min averages) measured by (b) the bottom-mounted ADCP, (c) Wave Glider Stokes, (d) Wave Glider Planck, and (e) Wave Glider WHOI43. White regions in (c)–(e) correspond to bands of interference from the Wave Glider subs; colored bars within the upper white band in each panel indicate the period when the corresponding Wave Glider occupied the central transect.

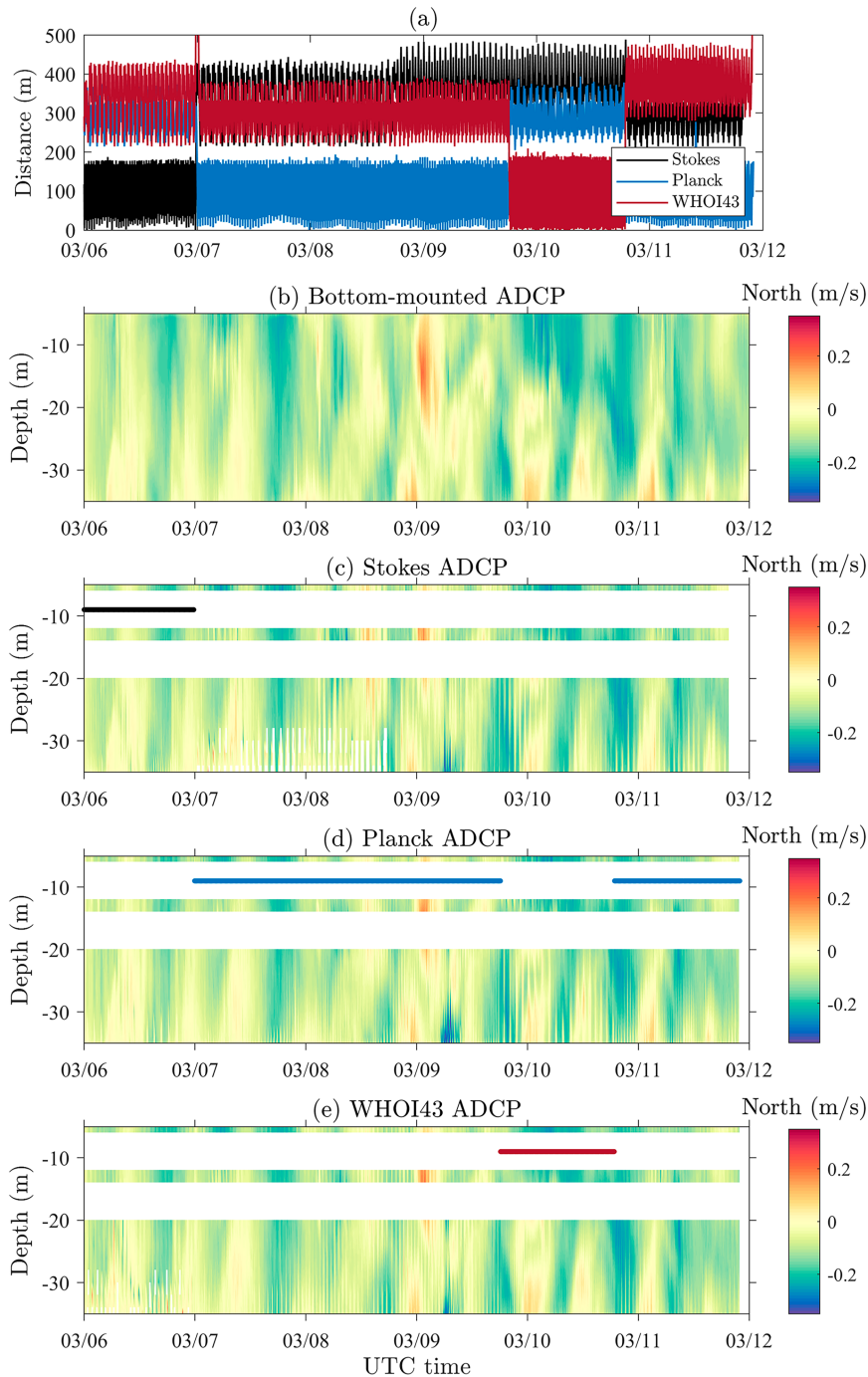


FIG. 5. As in Fig. 4, but for the north component of the current.

The Wave Gliders move continuously, so each ensemble average includes samples from a range of locations relative to the bottom-mounted ADCP; thus, some fraction of the difference in current reported from the two platforms is likely a result of natural spatial variability. As our goal is to accurately characterize instrumental errors in velocity observations made from the Wave Gliders, we wish to minimize the

confounding contribution of this natural variability; our examination of the discrepancy between Wave Glider-measured velocities and those from the bottom-mounted ADCP is therefore confined to periods of time—indicated by colored lines adjacent to the velocity component records in Figs. 4 and 5—when the Wave Glider in question was on the central transect (see Fig. 1). To further minimize the impact of spatial

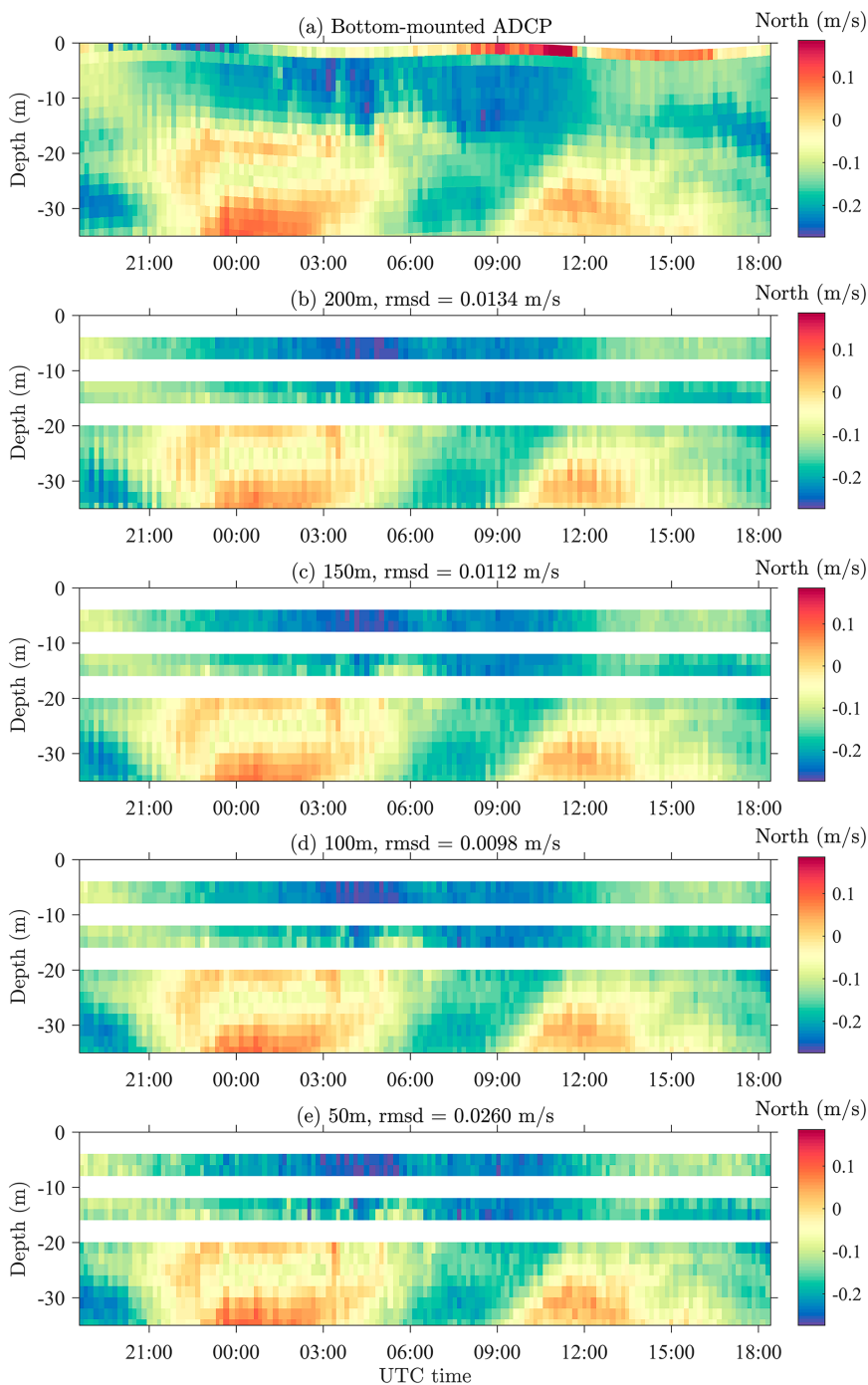


FIG. 6. (a) North component of the current measured from the bottom-mounted ADCP, with 10-min averaging. Also shown is the north component of the current measured from Wave Glider WHOI-43, also with 10-min averaging, and including only 1-Hz samples collected within a distance of (b) 200, (c) 150, (d) 100, and (e) 50 m of the bottom-mounted ADCP. RMS differences from (a) are given in the labels of (b)–(e). Note that, of these lower four panels, (d) appears to be smoothest and differs the least from (a), the bottom-mounted ADCP record.

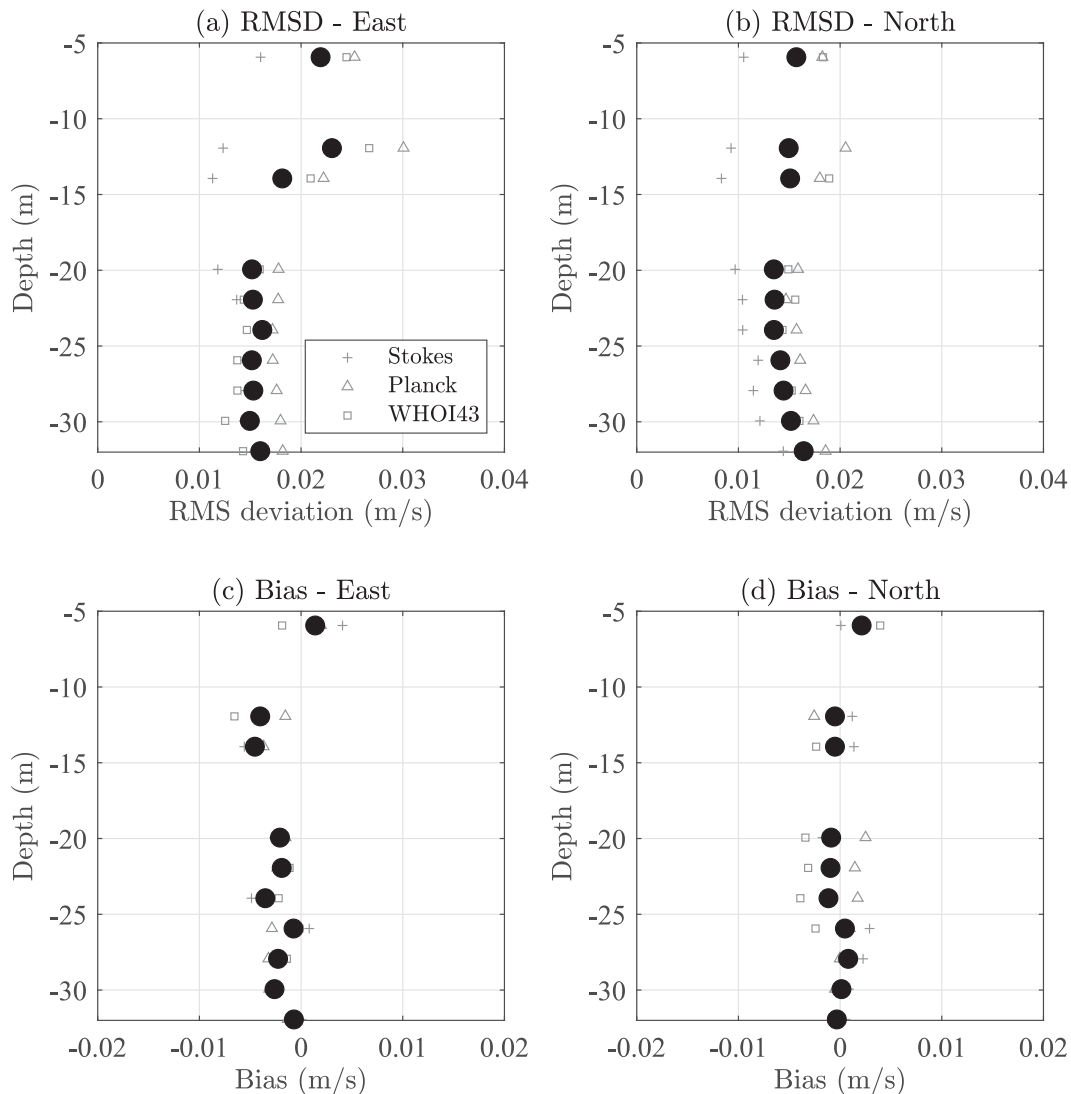


FIG. 7. (a),(b) RMS deviation and (c),(d) biases of the (left) east and (right) north current components for each of the three vehicles as a function of depth, using the GPS/IMU approach to platform motion correction. The black filled circles indicate the mean error value across all three vehicles.

variability, we restrict the samples included in each 10-min ensemble to those collected within a horizontal distance of 100 m from the bottom-mounted ADCP. This threshold distance represents the best compromise (Fig. 6): with larger thresholds (e.g., Fig. 6a), the discrepancy between measurements grows due to spatial variability, while with smaller thresholds, it grows due to random noise associated with smaller sample sizes (e.g., Fig. 6e).

Wave Glider Stokes occupied the central transect for the first day: between 2015 UTC 5 and 2345 UTC 6 March, this vehicle completed 52 round trips (~15 min per one-way transect). Wave Glider Planck occupied the transect for the following three days: between 0015 UTC 7 and 1745 UTC 9 March, it completed 116 round trips (also ~15 min per one-way transect). Wave Glider WHOI43 then spent a day on the central transect,

completing 87 round trips between 1815 UTC 9 and 1845 UTC 10 March (~8 min per one-way transect). Wave Glider WHOI43 moved faster than the other vehicles, which had additional drag because of the subsurface thermistor chain. In total 504 passes over the Sea Spider are considered in the analysis.

Here our main goal is to characterize the error associated with the Wave Glider-based current measurements; as the difference, $\mathbf{U}_{\text{diff}} = \mathbf{U}_{\text{WG}} - \mathbf{U}_{\text{bot}}$ between the current velocities observed from the bottom-mounted ADCP \mathbf{U}_{bot} and from the motion-corrected Wave Glider ADCP \mathbf{U}_{WG} includes this error along with other, presumably uncorrelated, contributions (alluded to above and enumerated in detail below), $|\mathbf{U}_{\text{diff}}|$ can reasonably be taken as an upper bound on the magnitude of the error associated with the Wave Glider current measurements.

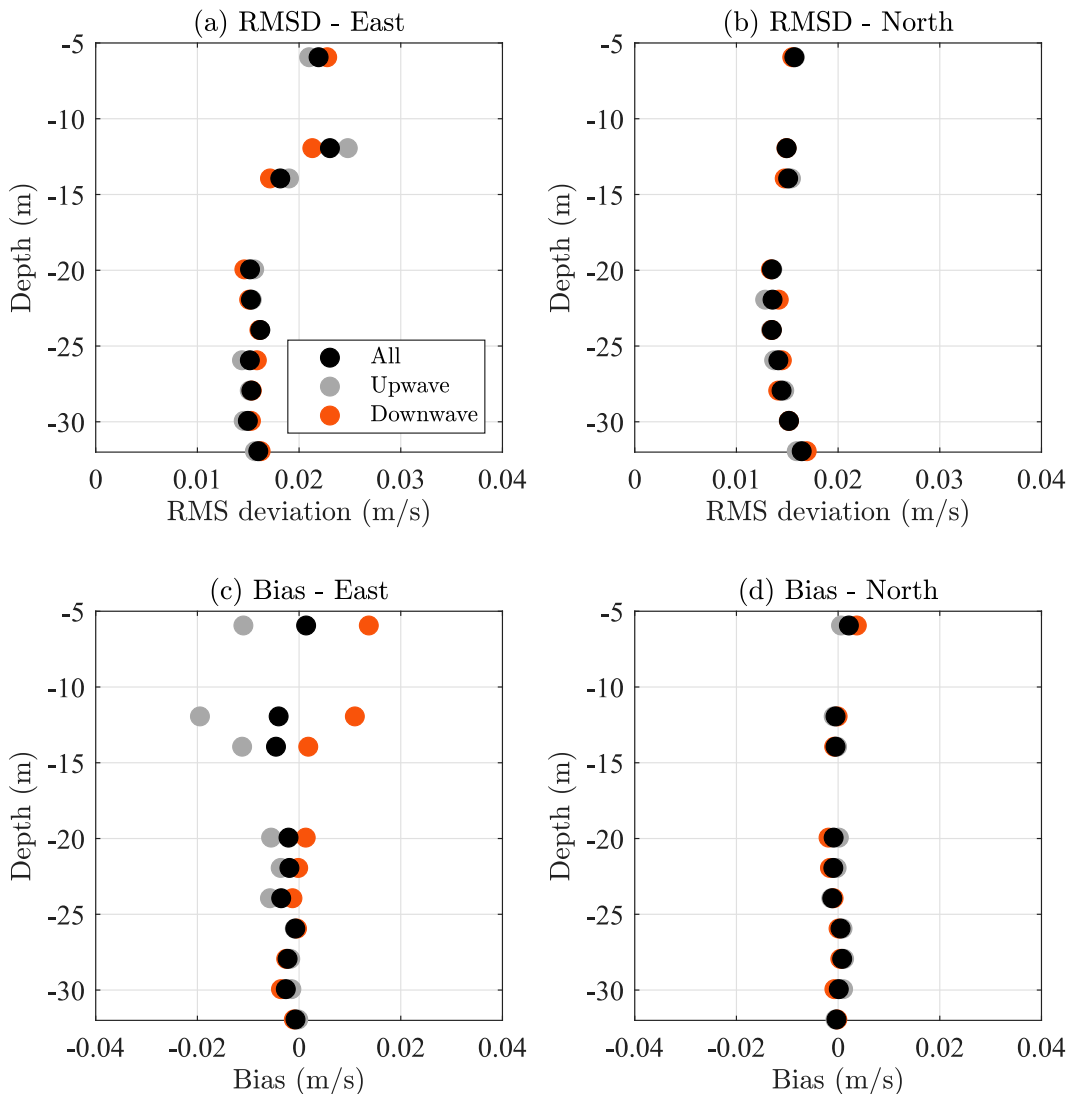


FIG. 8. Black filled circles (reproduced from Fig. 7): RMS deviation and bias, averaged across the three vehicles. Also shown are RMS deviation and bias when only samples from westward, or “upwave,” transects (gray filled circles) and only samples from eastward, or “downwave,” transects (red filled circles), are included. Note that near the surface there is a current measurement bias in the same direction as the Wave Glider’s course.

Differences between the current measurements made from the Wave Gliders and those made from the Sea Spider may arise from a number of sources, including the following:

- 1) Random noise inherent to the acoustic measurements made by both ADCPs. Block averaging in time is employed to reduce the impact of this noise. Nominal values for the standard deviation of single-ping noise of the instruments as configured were 8.77 cm s^{-1} for the Wave Gliders, and 4.32 cm s^{-1} for the Sea Spider; 600-ping (10 min at 1 Hz) ensemble averages would then be nominally subject to noise of 0.36 and 0.18 cm s^{-1} , respectively, for a nominal RMS discrepancy between ADCPs of 0.40 cm s^{-1} . In the case of the Wave Glider, there will be additional random noise in the inertial and GPS-based measurements of vehicle motion.
- 2) Natural variability. Because the Wave Gliders are moving, the 10-min averages of velocity include data that are not taken at the same location as the Sea Spider; natural spatial variability can thus cause differences between the Wave Glider velocity and the Sea Spider velocity. To minimize this effect, we only consider here the data collected from each Wave Glider during the period when it occupied the 300-m-long zonal transect centered directly over the Sea Spider, within 100 m of the Sea Spider.
- 3) Systematic bias in either current measurement. We anticipate some bias in average near-surface currents reported by the Wave Glider because the motion of the platform is correlated with the surface-wave-induced currents it measures. Bias could also result from imperfect motion/orientation correction. These errors are the primary concern motivating

the experiment described here, and our intention is to put bounds on them. However, systematic bias is also possible in the ADCP measurements made from the Sea Spider, particularly near the surface, where the four acoustic beams are most spread out (spanning ~ 30 m horizontally), the surface wave motion is most pronounced, and acoustic interference from the surface reflection is strongest; the surface degradation is apparent in Fig. 6a. Thus, while we generally consider the Sea Spider observations to represent “truth” and systematic differences between the two measurements to be “Wave Glider error,” in the upper few meters, a large fraction of the discrepancy is probably attributable to error in the measurement made from the Sea Spider. The large and variable “error” in the velocity from the first Wave Glider RDI range bin (~ 4 -m depth) must be interpreted accordingly; for the same reason, we focus here on validating the Wave Glider downward-looking current data against the record from the Sea Spider, leaving aside the upward-looking ADCP on the Wave Glider sub, which only samples the upper few meters.

For each of the horizontal current components (east and north) we consider the mean difference, or “bias,” and the root-mean-square (RMS) difference between the Wave Glider records and that from the Sea Spider as a function of depth, as shown in Fig. 7. The three vehicles show some difference in their error distributions (e.g., Stokes’s errors are generally smallest, perhaps due to the calmer conditions it experienced); in general, however, we find RMS errors at larger depths (roughly 20–30 m) in the range of $1\text{--}2\text{ cm s}^{-1}$, and biases of less than approximately 0.5 cm s^{-1} in magnitude (note, large black circles in Fig. 7 are averages across all three vehicles). The magnitudes of the bias and RMS differences increase near the surface, likely due to wave-induced errors in the bottom-mounted ADCP observations. Errors also increase at the deepest depths, where acoustic interference from the sea floor degrades the ADCP observations from the Wave Gliders.

To reveal any heading- or course-dependent biases, we also consider the errors observed during eastbound and westbound transits separately (Fig. 8). We find similar RMS error in both current components as well as a similar bias in the north current component, regardless of transit direction. Bias in the east component of the current, however, is much larger near the surface (12 m and shallower) with average errors greater than $+1\text{ cm s}^{-1}$ for the eastward transits, and -1 cm s^{-1} on westward transits. During the experiment, swell coming from the west was observed; it is possible that this bias arises from a slight correlation between the phase of the swell (and thus the observed wave orbital velocity) and the likelihood that a velocity sample will be rejected as poor quality due to low correlation of the acoustic return.

The most common method employed to motion compensate current profiles collected from Wave Gliders has relied on a combination of a tilt sensor and fluxgate compass, often located within and logged by the ADCP itself, to establish the instrument orientation needed to rotate the observed currents

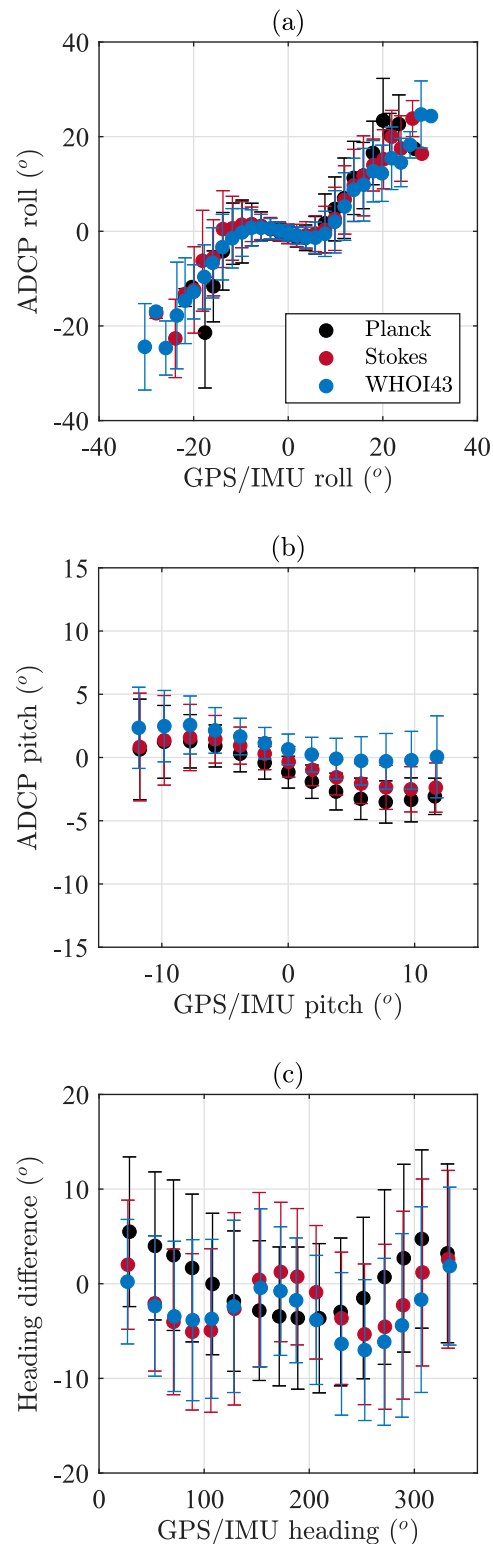


FIG. 9. (a) Roll reported by the ADCP vs roll reported by the GPS/IMU, (b) pitch reported by the ADCP vs pitch reported by the GPS/IMU, and (c) difference in reported heading (ADCP – GPS/IMU) vs heading reported by the GPS/IMU.

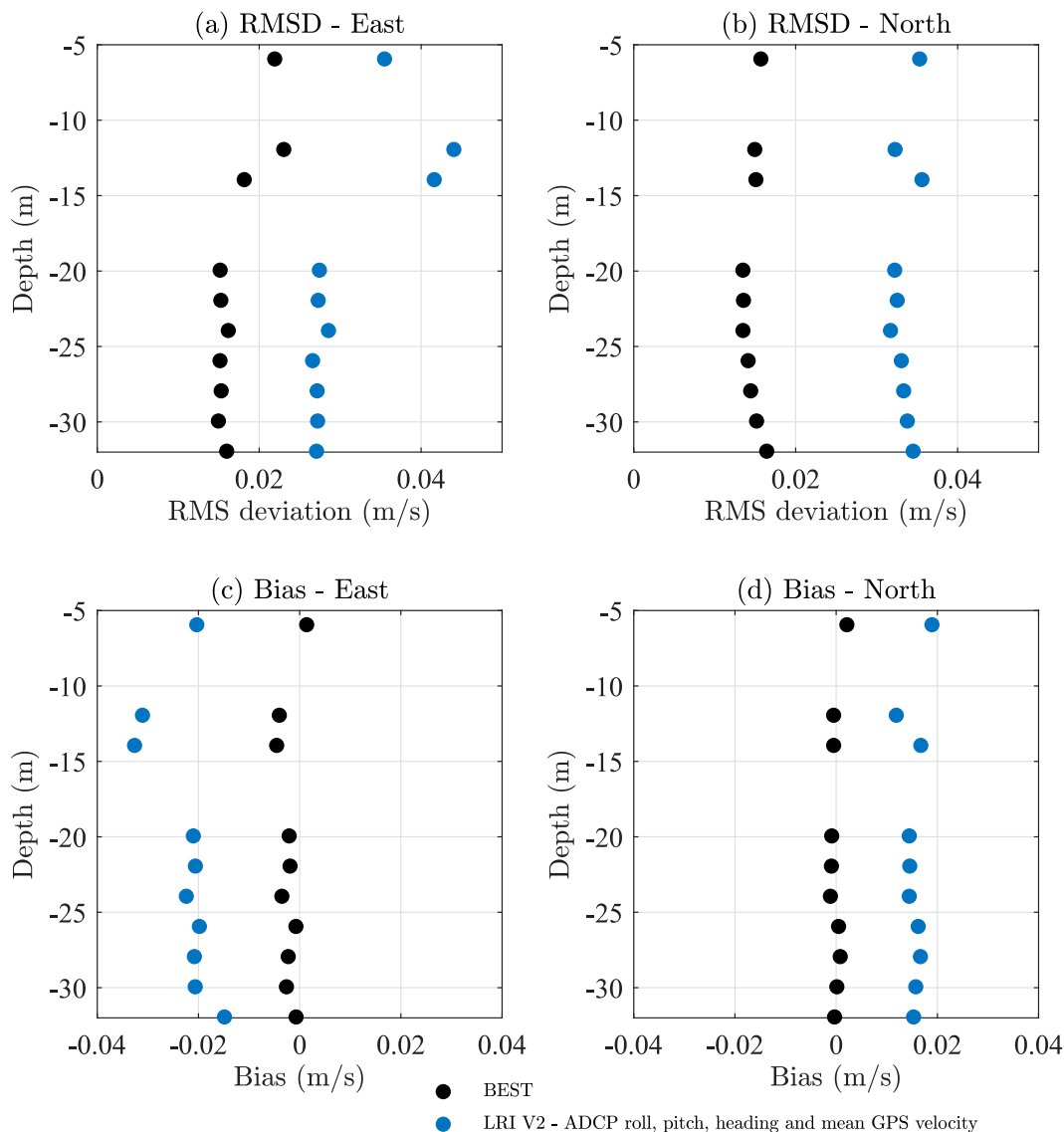


FIG. 10. (a),(b) RMS deviation and (c),(d) biases for the (left) east and (right) north current components as a function of depth, using the GPS/IMU approach to correct for platform motion [black filled circles (reproduced from Fig. 7)] and using the ADCP-measured attitude angles to rotate the observed current vectors and the mean GPS velocity to compensate for horizontal translation of the platform, similar to the standard LRI processing method (blue filled circles).

into the Earth-coordinate frame. We will refer to it as the “LRI” method in the following, since it is the standard onboard processing option provided by Boeing Liquid Robotics, developed during early Wave Glider ADCP integrations (Mullison et al. 2011). Given the typically large variation in vehicle attitude on time scales of $O(1)$ s, this operation must be carried out for each ping. Correction for horizontal translation of the platform, on the other hand, has commonly been applied as a single offset, based on GPS records, to an ensemble average current profile; GPS-derived velocities (as opposed to GPS/IMU derived velocities) are too noisy on short time scales to be used profitably for ping-by-ping

correction. A difference can arise between the mean platform velocity over the ensemble period and the mean of the 1-Hz velocity corrections when some acoustic returns must be rejected due to, for example, interference from bubbles. Because onboard ADCP tilt sensors respond to the lateral accelerations produced by ocean waves, the instantaneous pitch and roll angles they report differ significantly from the higher-fidelity output of an IMU (Fig. 9); for angles less than 10° , the pitch and roll from the two sources are actually anticorrelated. Dual-antenna GPS headings are more accurate than those produced by a fluxgate compass as well (Fig. 9c presents the difference in reported heading as a function of

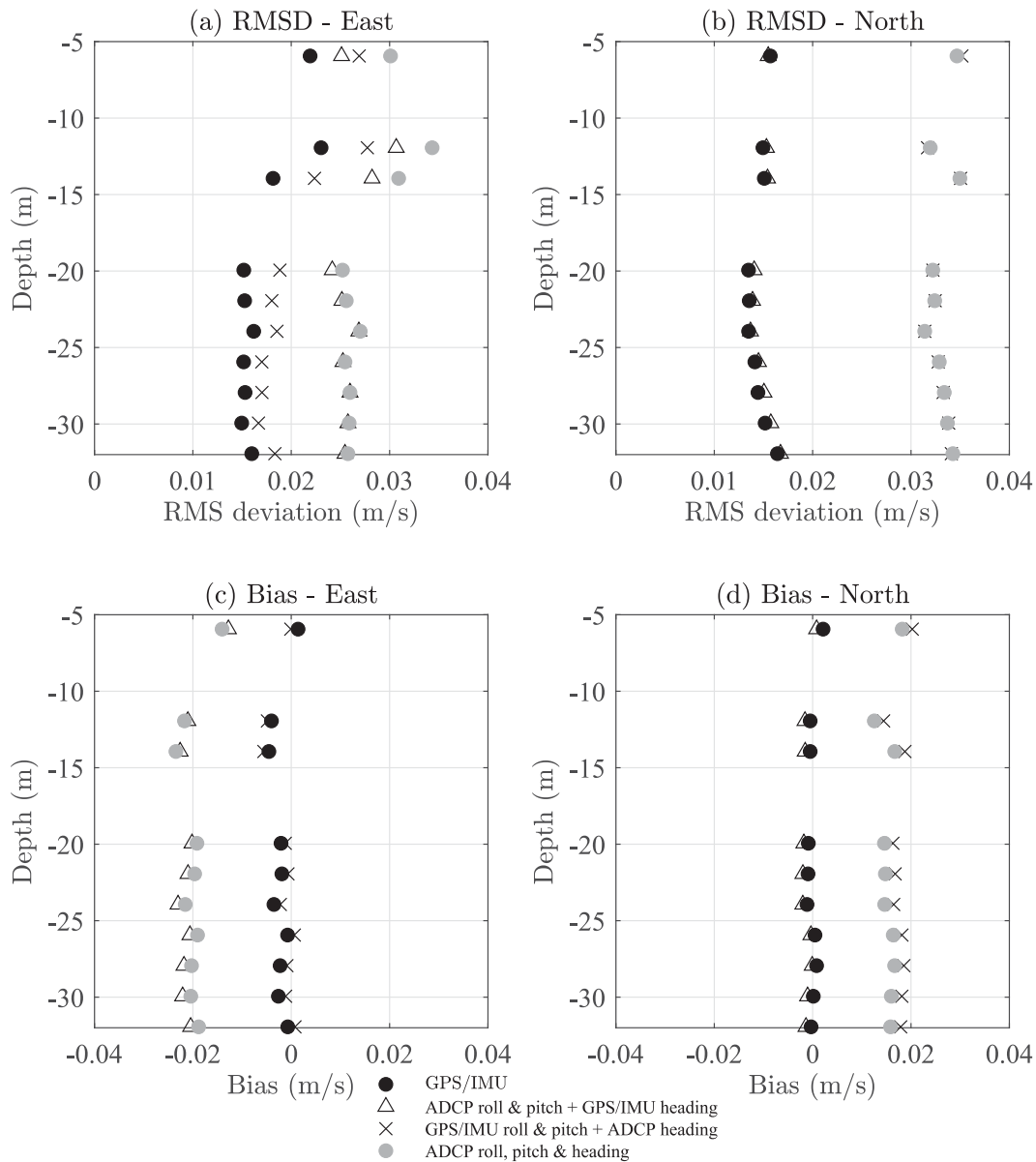


FIG. 11. (a),(b) RMS deviation and (c),(d) biases for the (left) east and (right) north current components using the GPS/IMU-derived platform velocity for motion correction [black filled circles (reproduced from Fig. 7)] and the cases when roll and pitch from the ADCP are used in place of those from the GPS/IMU (open triangles); when heading from the ADCP is used (crosses); and when pitch, roll, and heading from the ADCP are used (filled gray circles).

heading). Thus, there are a number of potential sources of additional error associated with the LRI method relative to the GPS/IMU method; in our experiment, these additional errors approximately double the RMS difference from the bottom-mounted ADCP record, from ~ 1.5 to $\sim 3 \text{ cm s}^{-1}$, and introduce biases of $\sim 2 \text{ cm s}^{-1}$ (Fig. 10).

The impacts on current observations due to 1) difference in the accuracy of pitch and roll measured by the ADCP relative to that measured by the GPS/IMU, 2) difference in the accuracy of heading reported by the two instruments, and 3) correction method for platform translation—ping-by-ping

GPS/IMU velocity versus ensemble mean GPS velocity—are presented in Fig. 11. Starting with 1 and 2, we calculate RMS differences and biases relative to the bottom-mounted ADCP record using GPS/IMU heading and ADCP pitch/roll; GPS/IMU pitch/roll and ADCP heading; and ADCP pitch, roll, and heading. In all three cases, platform translation is corrected for each ping with the GPS/IMU velocity. Each of these combinations results in biases and RMS errors that are noticeably larger than the GPS/IMU-corrected product (Fig. 11): using ADCP pitch and roll (triangles in Fig. 11) introduces substantial additional RMS deviation and bias in the east component of the current;

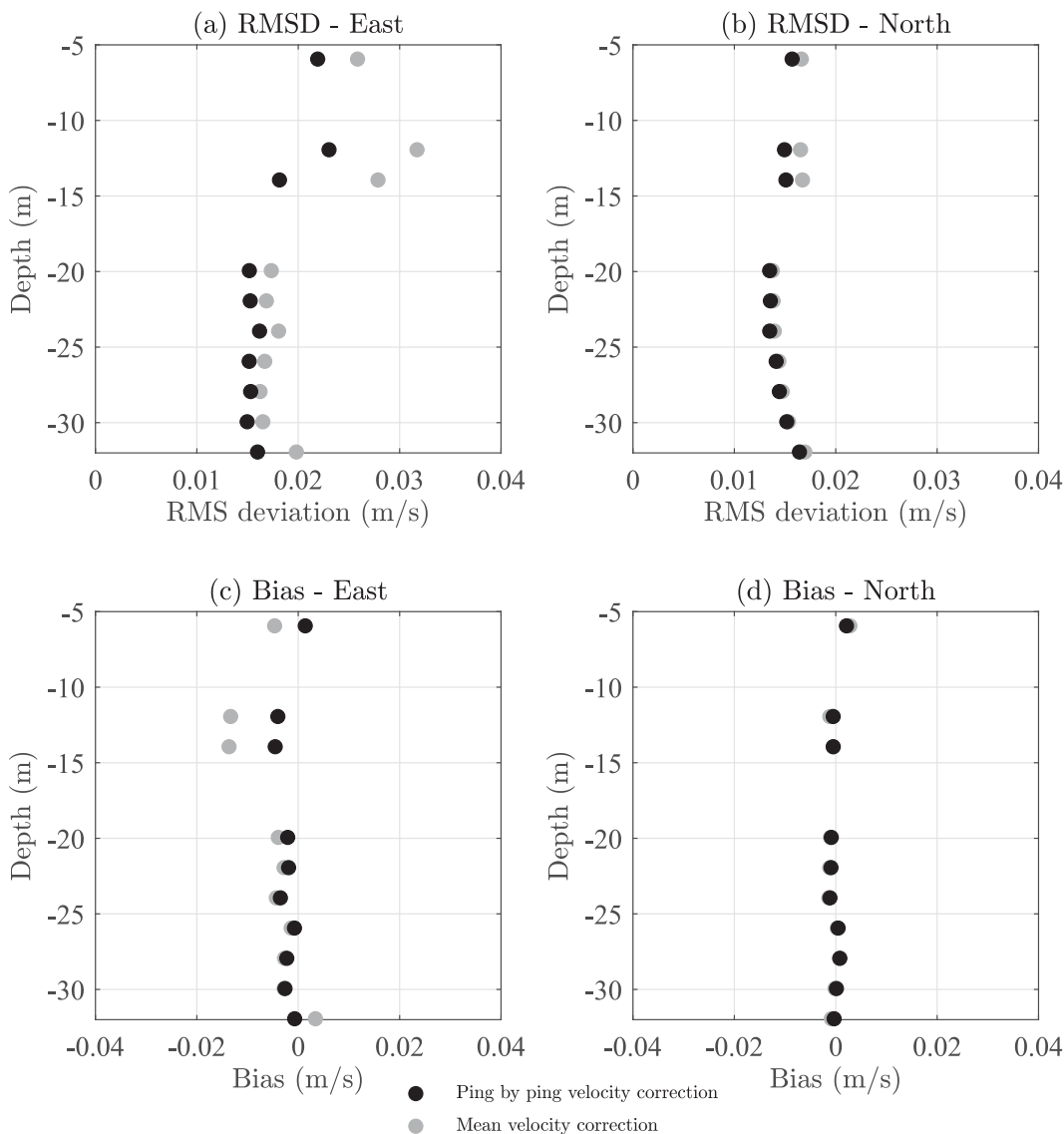


FIG. 12. (a),(b) RMS deviation and (c),(d) biases for the (left) east and (right) north current components as a function of depth, applying a platform velocity correction to each ping [black filled circles (reproduced from Fig. 7)] and: when using the mean Wave Glider velocity over the 10-min ensemble period to correct the current velocity for horizontal translation of the ADCP (gray filled circles).

using ADCP heading (α) adds significantly to the RMS deviation and bias in the north component, and also increases the RMS deviation of the east component somewhat at the shallower depths. The current velocity motion compensated using the onboard ADCP pitch, roll, and heading has substantially larger errors than the GPS/IMU-corrected current at all depths, for both north and east directions. Overall, we find significant improvement in the accuracy of current observations processed using the more accurate pitch, roll, and heading collected from the GPS/IMU sensor, and that neither more accurate pitch/roll alone, nor more accurate heading alone is sufficient to achieve the best accuracy.

The impact of using ensemble mean velocity versus ping-by-ping GPS/IMU velocity correction (item 3 above) is limited, at

least in this experiment (see Fig. 12). We find the largest errors in the east current component, primarily closest the surface, where the wave orbital speeds are largest.

5. Summary

In this work, we characterize the accuracy of Wave Glider-based ADCP measurements by comparing them with coincident (within 10 min) observations collected from a collocated (within 100 m) bottom-mounted ADCP over the course of a week-long experiment. Although Wave Gliders were the only vehicles examined in this study, the findings are likely relevant to other surface vehicles of similar size (e.g., Saildrones).

Aside from the methods described for ADCP alignment calibration, the results may also be applicable to observations made from similarly equipped mooring buoys. Characterizing the accuracy of current profile observations collected from such small floating platforms is necessary to estimate errors in vertical velocities inferred from their horizontal divergence, crucial to begin unraveling the role of submesoscale ocean dynamics in upper-ocean vertical transport.

A novel motion compensation method, tailored to wave-following surface vehicles that can experience significant motion under the action of surface waves, is presented and compared with the standard processing approach currently implemented in LRI Wave Glider platforms. We present a new heading alignment calibration method that enables calibration without independent current observations or ADCP bottom tracking, by minimizing covariance of Wave Glider heading with horizontal components of the measured current, an important step in improving their accuracy. We confirm that the onboard attitude sensor (tilt sensor) installed in the ADCP is not well suited to collect meaningful observations on small floating platforms at typical ADCP sampling frequencies [$O(1\text{ Hz})$], requiring the inclusion of a GPS/IMU on the vehicle to most accurately motion compensate the ADCP observations. Overall, we find significant improvements in the accuracy of the current observations as compared with the LRI method, with RMS errors at larger depths (roughly 20–30 m) in the range of 1–2 cm s^{-1} , and biases of less than approximately 0.5 cm s^{-1} in magnitude.

Note that we have here neglected a velocity bias relative to the Eulerian record collected from the bottom-mounted instrument arising from the vertical displacement of the platform (and thus the ADCP range bins) in conjunction with the wave motion of the water. This bias, analogous to the Stokes drift, is small at the depths we focus on in this work, but cannot be ignored closer to the surface, in particular in observations collected from the upward looking ADCP; they will be explored in a follow-up study.

Acknowledgments. The authors are grateful to Brett Pickering, the captain of the R/V *Beyster*, and to the diving crew Rich Walsh and Mohammad Sedarat for their support during the deployment and recovery of the Sea Spider and the Wave Gliders. Three anonymous reviewers provided valuable comments, improving the paper. This research was

supported by ONR (Grant N00014-19-1-2635) and NASA (Grant 80NSSC19K1688).

Data availability statement. The data used in this paper are available online (https://smode.whoi.edu/BTMA_2021/index.html).

REFERENCES

- Amador, A., S. Jaramillo, and G. Pawlak, 2017: ADCP bias and Stokes drift in AUV-based velocity measurements. *J. Atmos. Oceanic Technol.*, **34**, 2029–2042, <https://doi.org/10.1175/JTECH-D-16-0182.1>.
- , S. T. Merrifield, and E. J. Terrill, 2023: Assessment of atmospheric and oceanographic measurements from an autonomous surface vehicle. *J. Atmos. Oceanic Technol.*, **40**, 305–326, <https://doi.org/10.1175/JTECH-D-22-0060.1>.
- D’Asaro, E. A., and Coauthors, 2018: Ocean convergence and the dispersion of flotsam. *Proc. Natl. Acad. Sci. USA*, **115**, 1162–1167, <https://doi.org/10.1073/pnas.1718453115>.
- Farrar, J. T., and Coauthors, 2020: S-MODE: The Sub-Mesoscale Ocean Dynamics Experiment. *2020 IEEE Int. Geoscience and Remote Sensing Symp.*, Waikoloa, HI, IEEE, 3533–3536, <https://doi.org/10.1109/IGARSS39084.2020.9323112>.
- Grare, L., N. M. Stom, N. Pizzo, and L. Lenain, 2021: Instrumented Wave Gliders for air-sea interaction and upper ocean research. *Front. Mar. Sci.*, **8**, 664728, <https://doi.org/10.3389/fmars.2021.664728>.
- Hine, R., S. Willcox, G. Hine, and T. Richardson, 2009: The Wave Glider: A wave-powered autonomous marine vehicle. *OCEANS 2009*, Biloxi, MS, IEEE, <https://doi.org/10.23919/OCEANS.2009.5422129>.
- Lenain, L., and W. K. Melville, 2014: Autonomous surface vehicle measurements of the ocean’s response to Tropical Cyclone Freda. *J. Atmos. Oceanic Technol.*, **31**, 2169–2190, <https://doi.org/10.1175/JTECH-D-14-00012.1>.
- McWilliams, J. C., 2016: Submesoscale currents in the ocean. *Proc. Roy. Soc.*, **472A**, 20160117, <https://doi.org/10.1098/rspa.2016.0117>.
- Mullison, J., D. Symonds, and N. Trenaman, 2011: ADCP data collected from a Liquid Robotics Wave Glider. *2011 IEEE/OES 10th Current, Waves and Turbulence Measurements*, Monterey, CA, IEEE, 266–272, <https://doi.org/10.1109/CWTM.2011.5759563>.
- Pollard, R., 1973: Interpretation of near-surface current meter observations. *Deep-Sea Res. Oceanogr. Abstr.*, **20**, 261–268, [https://doi.org/10.1016/0011-7471\(73\)90015-6](https://doi.org/10.1016/0011-7471(73)90015-6).